Williamsburg, Virginia
ACTIVE 04
2004 September 20-22

Fluidic Chevrons for Jet Noise Reduction

Kevin Kinzie, Brenda Henderson
NASA Langley Research Center, Hampton, VA 23681

Julia Whitmire, Amal Abeysinghe
Goodrich Aerostructures Division, Chula Vista, CA, 91910

ABSTRACT

Chevron mixing devices are used to reduce noise from commercial separate-flow turbofan engines. Mechanical chevron serrations at the nozzle trailing edge generate axial vorticity that enhances jet plume mixing and consequently reduces far-field noise. "Fluidic chevrons" generated with air injected near the nozzle trailing edge create a vorticity field similar to that of the mechanical chevrons and allow more flexibility in controlling acoustic and thrust performance than a passive mechanical design. In addition, the design of such a system has the future potential for actively controlling jet noise by pulsing or otherwise optimally distributing the injected air. Scale model jet noise experiments have been performed in the NASA Langley Low Speed Aeroacoustic Wind Tunnel to investigate the fluidic chevron concept. Acoustic data from different fluidic chevron designs are shown. Varying degrees of noise reduction are achieved depending on the injection pattern and injection flow conditions. CFD results were used to select design concepts that displayed axial vorticity growth similar to that associated with mechanical chevrons and qualitatively describe the air injection flow and the impact on acoustic performance.

1. INTRODUCTION

As federal and local noise regulations are becoming stricter, noise characteristics are becoming more of a driving factor in aircraft engine design. At the same time, thrust performance and fuel efficiency requirements are also more important than ever. For most aircraft, the engine exhaust jet is typically a dominant noise source at one or more of the FAA noise metric certification points. Generally, reducing jet noise while maintaining thrust performance levels leads to conflicting system requirements. In addition, noise reduction is usually required only during operations close to the airport and only during a very short duration of the aircraft mission. Most jet noise reduction techniques are passive in nature and introduce thrust performance penalties over the entire aircraft mission rather than only when noise reduction is needed. Therefore, noise reduction techniques that are actively controlled and only implemented when necessary are of great value.

Various methods of mixing the jet plume for noise reduction have been tried in the past with varying degrees of success[1-4]. Many of the best mixing devices have inherently high associated thrust loss because momentum is usually lost from the exhaust flow while initiating the mixing process inside or at the exit of the nozzle. In addition, if the mixing generates too much small-scale turbulence, a detrimental increase in high frequency noise may result.

Chevron mixing devices are a relatively recent development that are being implemented on aircraft engines to provide jet noise reduction. They were developed during the NASA Advanced Subsonic Transport program[5] and subsequently further developed and implemented by industry[3] as mixing devices capable of providing noise reduction with minimal thrust loss. Figure 1 shows a picture of mechanical chevrons tested on a $1/9^{th}$ scale bypass ratio (BPR) 5 nozzle system tested in the NASA Langley Low Speed Aeroacoustic Wind Tunnel (LSAWT). By properly designing the chevron, enough vorticity can be generated to mix the jet flow, reduce the high-speed jet plume, and thereby reduce low frequency jet noise without producing too much small-scale turbulence that increases high frequency noise levels. Vorticity is generated by penetrating the chevron tip a small distance into the flow. While properly designed chevrons can minimize the associated thrust loss, penetrating chevrons into the flow during the entire aircraft mission

produces a loss in cruise performance. Recent work has been published on variable geometry chevrons[6] using smart materials, but the high temperature of the core flow region currently limits such an application to the cooler fan nozzle flow.

The chevron vorticity field in the jet plume is responsible for mixing the core and fan flows and producing noise reduction. Therefore, it may be possible to generate a vorticity field similar to that of the chevron using a different technique, such as injecting air at the nozzle trailing edge, and produce a similar reduction in noise. An air injection system could be implemented on either the fan or core nozzles and have the added advantage of being actively controlled and only used when necessary.

This paper reports results from an investigation using air injection as "fluidic chevrons" for use on separate flow nozzles. An approximate $1/9^{th}$ scale BPR 5 nozzle system was designed and tested in NASA Langley's Low Speed Aeroacoustics Wind Tunnel. Pretest CFD screening of candidate nozzle configurations was performed and the results were qualitatively evaluated to aid the nozzle design. Acoustic measurements show that noise reduction was achieved by the air injection technique.

2. EXPERIMENTAL APPROACH

The LSAWT is a continuous flow in-draft wind tunnel that provides a free jet surrounding a Jet Engine Simulator (JES) exhaust flow. A schematic of the facility is shown in Figure 2. The JES produces two coannular streams to accurately simulate engine nozzle systems. The JES has two propane-fired, sudden-expansion burners that produce fan and core nozzle streams with actual engine temperatures and pressures. Each stream can flow air up to a maximum of 7.7 kg/sec. In addition, each stream has an electric pre-heater for low temperature operation and burner stability. Airflow is straightened through turbulence management devices before transitioning to the nozzle and is measured by critical flow venturi meters in each stream. Pressure and temperature rakes are positioned just upstream of the nozzle contraction to measure nozzle operating conditions. The free jet is produced by a 1.43 meter square nozzle. Wind tunnel speed can be varied from a Mach number (Mfj) of 0.1 up to 0.32. The test section has anechoic treatment from fiberglass wedges and the cut-off frequency is 250 Hz. Dimensions of the test cell, measured from tip-to-tip of the wedges is 10.36 meters long by 5.18 meters high by 5.18 meters wide. The downstream flow collector regulates flow recirculation in the test cell. Both the wind tunnel nozzle and the flow collector are acoustically treated to minimize reverberations.

Acoustic data were collected with a 28 microphone sideline array located 3.52 meters from the centerline axis of the model. Directivity angles (θ) less than 90^o are in the forward quadrant towards the upstream jet axis and angles greater than 90^o are towards the downstream jet axis in the aft quadrant. Microphones were ¼" diameter, operated with the grid caps removed, and calibrated with a piston phone and electrostatic calibrator before and after the test. Acoustic data are processed to 1/3 octave bands and include corrections for the microphone calibration, wind tunnel background noise, a Doppler shift to the spectral data, and atmospheric absorption to acoustic standard day conditions using the Shields and Bass[7] methodology. The Amiet point source[8] shear layer correction model is used to account for acoustic propagation through the free jet shear layer. The data shown here are scaled to full-scale engine size using a scale factor of 1/9 and extrapolated to a distance of 543 meters which corresponds to an altitude of 305 meters and a ground sideline distance of 500 meters

For these experiments, a special BPR 5 nozzle system was designed that allows air to be injected near the core nozzle trailing edge. A low mass flow delivery system brings air to the core nozzle through the pylon and internal struts. The injection air is metered using a critical flow venturi meter and is capable of delivering up to 0.227 kg/s. The fluidic chevron model system is shown installed in the LSAWT in Figure 3. Figure 4 shows diagrams of the model and air delivery system. The model system has the same external flow lines for the fan nozzle, core nozzle, pylon, and centerbody as the NASA Propulsion Airframe Aeroacoustic (PAA) BPR 5.0 nozzle[9] except near the core nozzle trailing edge. The fluidic chevron core nozzle trailing edge is thickened relative to the PAA nozzle to accommodate air injection through a plenum inside the core nozzle structure. The air is injected through slots located on the core nozzle surface near the trailing edge as shown in Figure 5.

The extra thickness of the nozzle trailing edge generated an unexpected strong tone in the acoustic data that was associated with the trailing edge tone effect described in Olsen and Karchmer[10] and more recently Henderson, Kinzie, and Haskin[11]. To eliminate the tone, a 0.005" thick shim 0.4" long was attached to the trailing edge surface on the outside of the core nozzle (also shown in Figure 5) to shield the thick base region and to prevent shedding of vortices responsible for the tone generation. Therefore, the slots were

effectively located 0.4" farther from the trailing edge than originally intended. While this technique eliminated the trailing edge tone, indications from the CFD analysis showed that moving the slots away from the trailing edge reduced the mixing and hence possibly the noise reduction as well. However, the shimmed configuration was deemed preferable to the strong tone and was used during the entire test.

Several interchangeable hollow core nozzle trailing edge parts were fabricated and tested. The nozzles attached to the model system as shown in Figure 4. The inner and outer core nozzle surfaces were sealed to prevent air leakage from inside the nozzle plenum into the air streams. A choke plate located in the nozzle plenum provided uniform flow around the circumference of the plenum and through the slots. Four equally spaced total pressure tubes around the circumference measured the pressure downstream of the choke plate in the nozzle plenum and showed the pressure in the plenum chamber was normally within 0.5% at each azimuthal location for all injection pressure conditions indicating very uniform flow from each of the injection slots.

Configurations tested are listed in Table 1 and include both "inflow" and "alternating" injection patterns. For the "inflow" pattern, all slots injected air through the nozzle surface into the core flow near the core nozzle trailing edge. For the "alternating" pattern, slots injected air into either the core or fan stream (i.e. for a given slot injecting into the core flow, the adjacent slots inject into the fan flow and vice versa). The "inflow" configurations had 6 and 8 surface slots evenly spaced about the circumference of the core nozzle while the "alternating" configurations had 8, 12, or 24 total slots. All slots were placed so as to avoid interference of the injected air with the pylon structure. Slot dimensions were determined based on CFD analysis as well as considerations for realistic constraints on total injected mass flow rate. The data reported here focuses only on the two "inflow" configurations.

Two engine cycle conditions representative of a typical BPR 5 engine at the takeoff and cutback noise certification points were tested. Only results for the takeoff condition (cycle point 15) are shown here. The conditions of the core and fan streams are shown in Table 2. In addition, two forward flight Mach numbers of 0.1 and 0.28 were tested. A range of injection pressure ratios was also tested. For proprietary reasons, the injection nozzle pressure ratio (NPR) is normalized to values between 0 and unity where 0 represents no injection flow and 1 represents the maximum injection NPR tested. The term NPR* is used here to represent the normalized pressure ratio.

3. NUMERICAL ANALYSIS

Prior to fabricating the hardware, many different air injection concepts were screened using computational fluid dynamics to investigate the mixing properties of various configurations. Development of the flow field for fluidic and mechanical chevrons was shown to be qualitatively similar. The analysis was conducted to determine a combination of parameters that would be effective in creating a mean flow field similar to that from a passive mechanical chevron nozzle. While a direct link between the flow field solution and radiated noise isn't possible at this time, qualitative analysis of the mean flow, turbulence, and vorticity fields can give an indication of which design parameters might have the most impact. For instance, locating the slots closer to the trailing edge demonstrated more mixing between the fan and core streams compared to slots located further inside the nozzle. Other parameters investigated in the 24 screening cases included number of slots, slot injection pattern, slot dimensions, total injected mass flow rate, slot injection pressure ratio, and slot spacing. Based on these CFD solutions, the five configurations shown in Table 1 were chosen for testing.

All computations were performed using the multi-block, parallel, structured code PAB3D[12]. The nozzle fluid flow and plume were simulated by solving the asymptotically steady, compressible, Reynolds-averaged, Navier-Stokes equations using an implicit, upwind, flux-difference splitting finite volume scheme. The turbulence model was a standard two-equation k-epsilon model with a linear stress representation. The computational domain extends over 30 core nozzle diameters (Dc) downstream of the fan nozzle exit in the streamwise direction and has a radial extent from 0 (centerline) to 6 Dc. All solutions are for a nozzle with no pylon even though a pylon was used in the experiment to bring the injection air into the core nozzle. Only a sector of the flow is modeled with symmetry boundary conditions in the azimuthal direction. The size of the sector modeled is determined by the number of slots. For configurations with 6 slots, a 30 degree sector is modeled; for configurations with 8 slots, a 22.5 degree sector is modeled. For all "inflow" configurations, the sector extends from the slot centerline to halfway between the slots.

For the screening CFD analysis, the internal injection flow through the core nozzle plenum was not modeled. Air injection through the slots in the core nozzle was modeled as a boundary condition on the portions of the inner core nozzle surface covering the injection slots. The slot boundary conditions were defined by setting injection flow total pressure, total temperature, and injection angle of flow at the slot exit. This boundary condition method is computationally simpler than modeling the injection flow plenum, but results in an overestimate of injection flow because real nozzle effects are not included. The simulation and test operating conditions are listed in Table 2. These operating conditions are similar to those reported in Thomas and Kinzie[9] and Thomas, Kinzie, and Pao[13] for passive mechanical chevrons.

Figures 6 (a-c) show total temperature, Tt, contours in the vertical centerline plane for the baseline, 8I, and 6I configurations. For the 8I and 6I cases, the normalized slot injection pressure ratio equals 0.36. In these plots, the freestream total temperature of 295K is set to the color black. From these plots, the length of the core jet potential core (Tt > 800 K shown in red) can be identified for each configuration. Comparison of Figures 6 (a-c) shows that the fluidic chevrons reduce the length of the core jet potential core relative to the baseline nozzle for both the 8I and 6I configurations. The potential core extends to approximately x = 15 Dc for the baseline nozzle, x = 13 Dc for the 8I configuration, and x = 10 Dc for the 6I configuration. These results indicate that, for the same injection pressure ratio, decreasing the number of slots results in increased mixing of the fan/ core shear layer. The decrease in potential core length from the fluidic chevrons is very similar to that of the passive mechanical chevrons shown in Thomas, Kinzie, and Pao[13].

As an indicator of mixing between the hot core flow and cooler fan flow, Figure 7 shows cross sections (planes normal to the streamwise direction) of jet total temperature for several downstream axial locations. Downstream locations of x/Dc = 2, 5, and 8 are shown for the baseline, 8I, and 6I configurations. For the injection configurations, the normalized slot injection pressure ratio equals 0.36. For these configurations, injecting air into the core flow results in the generation of a lobed pattern as core flow (Tt > 800K shown in red) is entrained into the fan flow (Tt < 350 K shown in blue). For the baseline nozzle, a distinct large region containing unmixed core flow can still be seen at x/Dc = 8. For the case with 6 injection slots, at x/Dc = 8, only a small region containing unmixed core flow still exists. The case with 8 injection slots shows significantly more mixing of the core flow with the fan flow at x/Dc = 8 than the baseline, but less than the case with 6 slots. Figure 7d shows the same total temperature cross-sections for an 8 serration mechanical chevron from Thomas, Kinzie, and Pao[13]. There are strong similarities in the details of how the lobes develop and mix the core and fan flow. Based on these results, the passive mechanical chevron design appears to mix the flow better than either fluidic chevron. However, differences in the CFD implementation and subtleties in the mean and turbulence fields make it difficult to perform a direct comparison.

4. RESULTS AND DISCUSSION

The overall sound pressure level (OASPL) directivity for the 8I nozzle at four air injection conditions is shown in Figure 8. The conditions are for cycle point 15 and forward flight Mach number of 0.10. Spectral data at representative aft, middle, and forward angles are shown in Figures 9-11. At the aft angles (greater than approximately $\theta = 110^o$), where the jet noise sources peak, there is a steady decrease in OASPL as the injection pressure is increased. The spectral plot at $\theta = 145^o$ (Figure 11) shows the overall reduction results from reduced low frequency noise components. Higher momentum of the injection flow leads to higher levels of vorticity generated in the jet as well as increased mixing between the core and fan streams thereby decreasing the low frequency noise sources in the plume. A similar effect is seen in passive mechanical chevron designs where higher levels of tip penetration also increases the mixing and low frequency noise reduction[4].

Towards the middle and forward directivity angles (less than approximately $\theta = 110^o$), however, there is less reduction in the OASPL. The spectral data show that the injection causes an increase in high frequency noise that can offset lower frequency noise reduction. In general, as the injection pressure is increased both the amount of low frequency attenuation and high frequency augmentation are also increased. It is not possible to determine from these data whether the high frequency increase is associated with increased small-scale turbulence levels from the mixing process or whether the interaction of the injection jets with the core flow is responsible for augmenting high frequency noise. As mentioned earlier, it is common for mixing devices to produce additional small-scale turbulence resulting in significant high frequency noise generation. Noise measurements of the injector jets alone show levels much less than the

combined fan and core jets. However, once the core flow is introduced, the interaction of the injection jets with the core flow creates a cross-stream jet configuration that might generate a significant amount of noise.

Figure 12 shows the OASPL for the 6I nozzle with the same range of injection pressure ratios as shown for the 8I with the Mach 0.10 forward flight condition. The trends for the 6I nozzle are very similar to those for the 8I nozzle. There is a steady decrease in peak jet noise as NPR* is increased. Representative spectral plots follow in Figures 13-15. The spectrum at $\theta = 145^o$ shows an even clearer dependence of low frequency noise reduction on the injection NPR. There is low frequency noise reduction at all angles, but a cross-over point around 500 Hz where high frequencies begin to increase is observed in the middle and forward angles.

The effect of forward flight was investigated by increasing the free jet Mach number to 0.28. Figure 16 shows the OASPL for the 6I nozzle for the higher free jet Mach number. The directivity shape changes considerably compared to the Mfj = 0.10 case due to the reduced shear between the fan stream and free jet as well as noise source convection effects. In spite of these changes, the aft angle noise reduction for the injection cases is still similar to that observed for Mfj = 0.10. However, the middle and forward angles now show the injection cases to actually be louder on an OASPL basis relative to the no injection flow case. The spectral data at $\theta = 90^o$ shown in Figure 17 reveals the cause of this trend reversal at the higher forward flight Mach number. The lower frequency regime is affected by forward flight more significantly than the higher frequency regime. The amount of high frequency augmentation from the injection over the baseline is comparable for both the lower and higher free jet Mach numbers. Therefore, the high frequency noise components contribute more to the OASPL for the higher free jet Mach number.

It is reasonable to assume that high frequency noise generated close to the core nozzle lip by the injection jets is less affected by forward flight than the lower frequency noise generated farther downstream by the jet plume due to the fact that the inner shear layer is unaffected by the free jet flow at this axial location. The low frequency components show a forward flight effect benefit resulting from the reduced shear between the jet and free stream as the free jet Mach number is increased. However, close to the core nozzle exit, the inner shear layer region between the fan and core flows is shielded from the effects of the free jet by the fan stream and little forward flight effect benefit is realized by the high frequencies generated in that region.

5. CONCLUSIONS

Actively controlled fluidic chevrons are shown to have the potential to reduce jet noise in a manner similar to more conventional passive mechanical chevron devices. The amount of noise reduction is a function of injection parameters such as number of injection slots and injection pressure ratio. Low frequency noise reduction is most likely the result of enhanced mixing between the fan and core streams as indicated by the CFD analysis. However, the addition of injection flow also increases the high frequency noise, which offsets the low frequency reduction in some cases. The exact cause of the high frequency augmentation is not yet known. Additional research is required to fully evaluate the noise reduction on an aircraft system level. Further optimization of fluidic chevrons may improve the noise reduction characteristics and offers the promise of actively controlling jet noise in an engine application.

6. ACKNOWLEDGEMENTS

The authors wish to thank the Jet Noise Laboratory staff for their many contributions to the planning, operation, and data processing required for the experiment that produced the results written in this paper. Jacky Yu and Harry Haskin are also acknowledged for leading the mechanical design of the model system.

7. REFERENCES

1. Zaman, K.B.M.Q., Reeder, M.F., and Samimy, M., "Control Of An Axisymmetric Jet Using Vortex Generators," *Physics of Fluids*, 6 (2), 778-793, 1994.
2. Seiner, J.M., and Grosch, C.E., "Mixing Enhancement by Tabs in Round Supersonic Jets," 4th AIAA/CEAS Aeroacoustics Conference, AIAA Paper 98-2326, 1998.
3. Martens, S., "Jet Noise Reduction Technology Development at GE Aircraft Engines," ICAS 2002 Congress, 2002.

4. Callender, B., Gutmark, E., and Martens, S., "A Far-field Acoustic Investigation into Chevron Nozzle Mechanisms and Trends," 41st Aerospace Sciences Meeting and Exhibit, AIAA Paper 2003-1058, 2003.
5. Saiyed, N.H., Bridges, J.E., and Mikkelson, K.L., "Acoustics and Thrust of Separate-Flow Exhaust Nozzles with Mixing Devices for High-Bypass-Ratio Engines," 6th AIAA/CEAS Aeroacoustics Conference, AIAA Paper 2000-1961, 2000.
6. T. L. Turner, R. D. Buehrle, R. J. Cano, and G. A. Fleming, "Modeling, Fabrication, and Testing of a SMA Hybrid Composite Jet Engine Chevron Concept," *2004 International Symposium on Active Control of Sound and Vibration*, INCE-USA, Williamsburg, VA, 20-22 September, 2004.
7. Shields, F. D. and Bass, H. E., "A Study of Atmospheric Absorption of High Frequency Noise and Application to Fractional Octave Bands of Noise," NASA Contractor Report 2760, 1976.
8. Amiet, R.K. Correction of Open Jet Wind Tunnel Measurements for Shear Layer Refraction. AIAA Paper 77-54, 1977.
9. Thomas, R.H., and Kinzie, K.W., "Jet-Pylon Interaction of High Bypass Ratio Separate Flow Nozzle Configurations," 10th AIAA/CEAS Aeroacoustics Conference, AIAA Paper 2004-2827, 2004.
10. Olsen, W. and Karchmer, A., "Lip Noise Generate by Flow Separation on Nozzle Surfaces," NASA TM X-71859, 1976.
11. Henderson, B.S., Kinzie, K.W., and Haskin, H.H., "The Effect of Nozzle Trailing Edge on Jet Noise," 10th AIAA/CEAS Aeroacoustics Conference, AIAA Paper 2004-2948, 2004.
12. Pao, S.P, and Abdol-Hamid, K.S., "Numerical Simulatoin of Jet Aerodynamics Using the Three-Dimensional Navier-Stokes Code PAB3D," NASA Technical Paper 3596, 1996.
13. Thomas, R.H., Kinzie, K.W., and Pao. S.P., "Computational Analysis of a Pylon-Chevron Core Nozzle Interaction," 7th AIAA/CEAS Aeroacoustics Conference, AIAA Paper 2001-2185, 2001.

Table I Injection nozzle configurations tested in the LSAWT

Configuration	# of Slots	Pattern
8I	8	Into Core
6I	6	Into Core
24A	24	Alternating
12A	12	Alternating
8A	8	Alternating

Table II Operating conditions for the CFD and experiment

Cycle Pt.	Core NPR	Core Total Temp.	Fan NPR	Fan Total Temp.
5	1.33	722° K	1.51	340° K
15	1.56	828° K	1.75	359° K

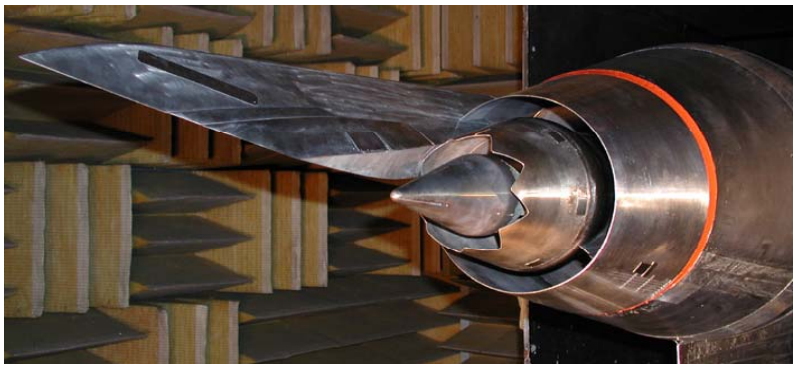

Figure 1 BPR 5 nozzle with eight-chevron core nozzle installed on the JES in the LSAWT.

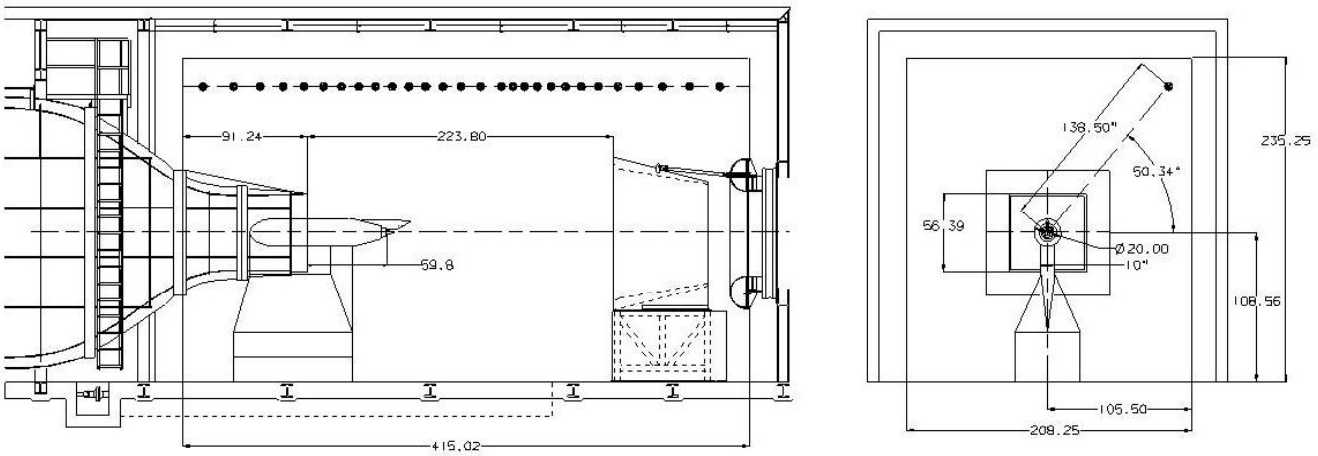

Figure 2 NASA Langley's Low Speed Aeroacoustic Wind Tunnel, side view of test section (left) with flow from left to right and end view looking upstream (right). Microphone array shown in upper right hand side of the end view. Dimensions in inches.

Figure 3 Fluidic chevron model installed in NASA Langley LSAWT facility.

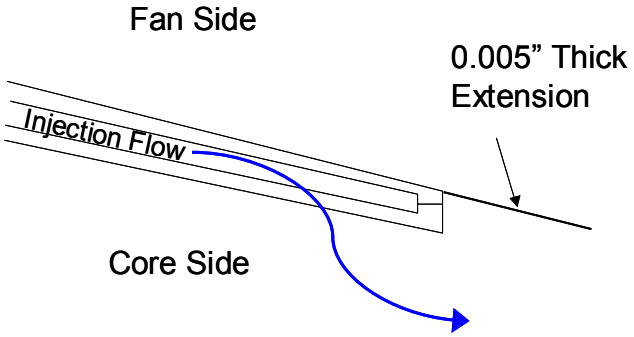

Figure 5 Schematic of surface slot injection into core flow near core nozzle trailing edge.

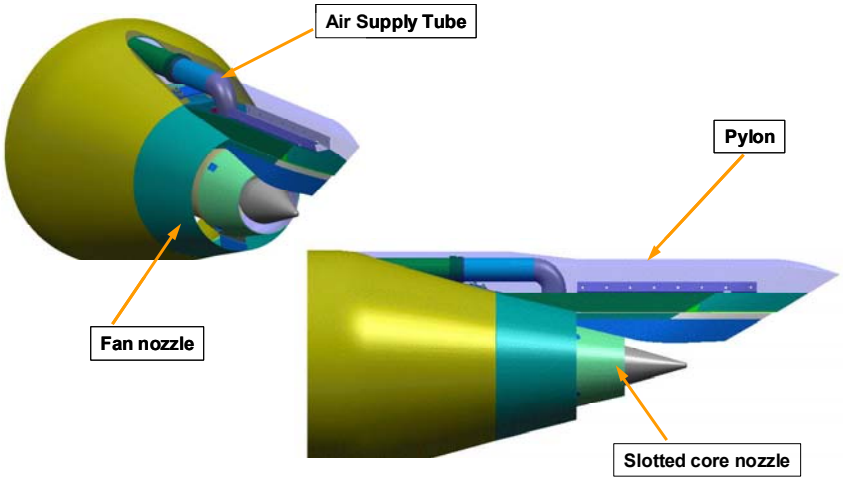

Figure 4 Schematics of fluidic chevron model system hardware.

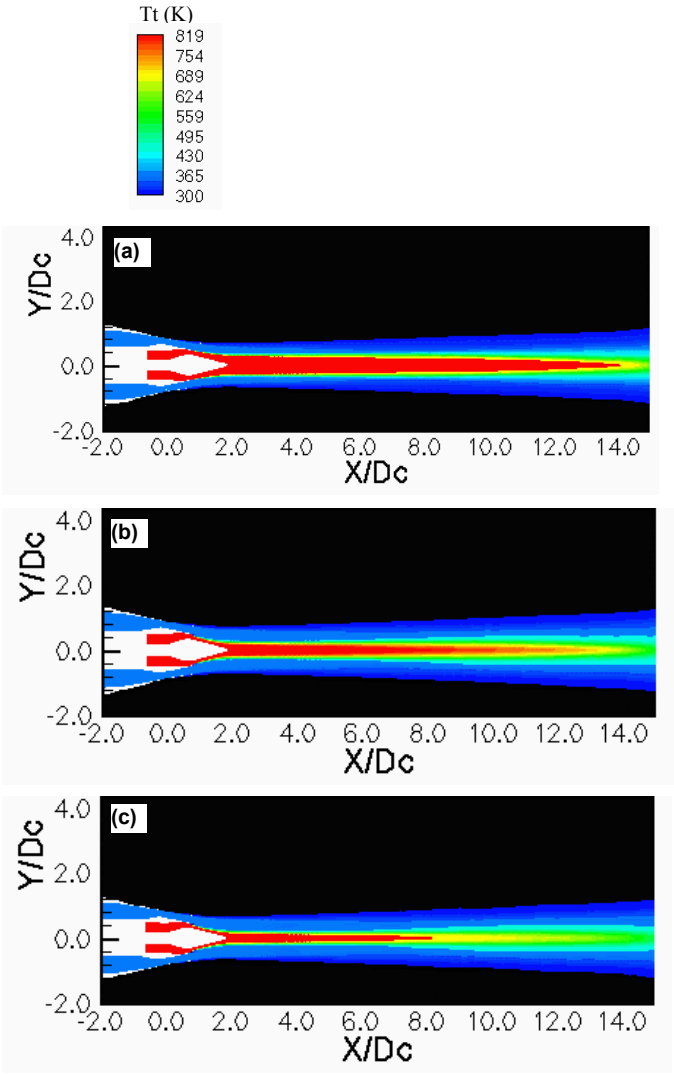

Figure 6 Centerline symmetry plane contour plot of total temperature from CFD simulations at cycle point 15. (a) round nozzle baseline configuration (b) fluidic chevron configuration with 8 slots injecting into core flow (8I) at NPR* = 0.36 (c) fluidic chevron configuration with 6 slots injecting into core flow (6I) at NPR* = 0.36.

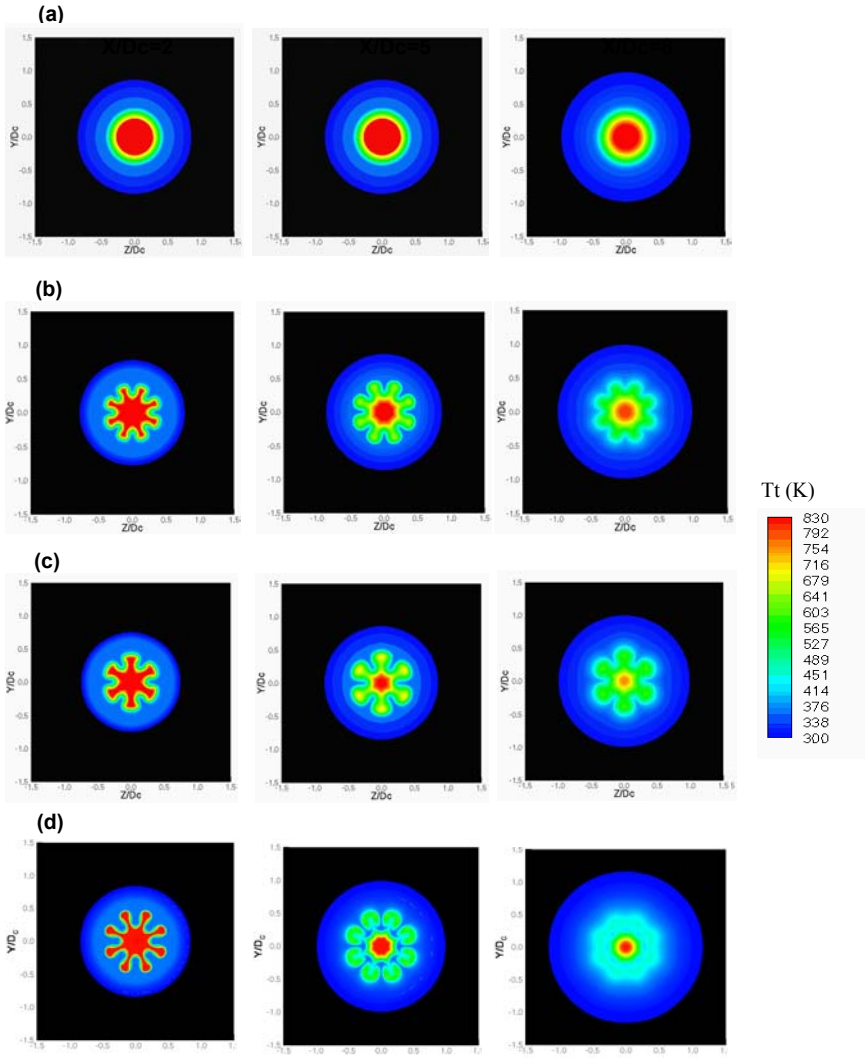

Figure 7 Downstream cross-section contour plots of total temperature from CFD simulations at cycle point 15 for axial locations at x/Dc of 2, 5, and 8. (a) baseline (b) fluidic chevrons with 8 slots injecting into core flow (8I) at NPR* = 0.36 (c) fluidic chevrons with 6 slots injecting into core flow (6I) at NPR* = 0.36 (d) mechanical chevrons with 8 core serrations (from reference 13).

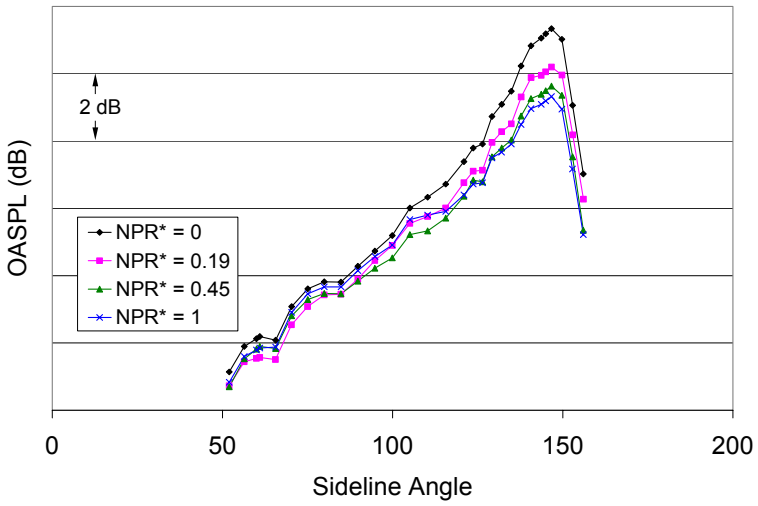

Figure 8 OASPL of 8I nozzle operating at cycle point 15, Mfj = 0.10.

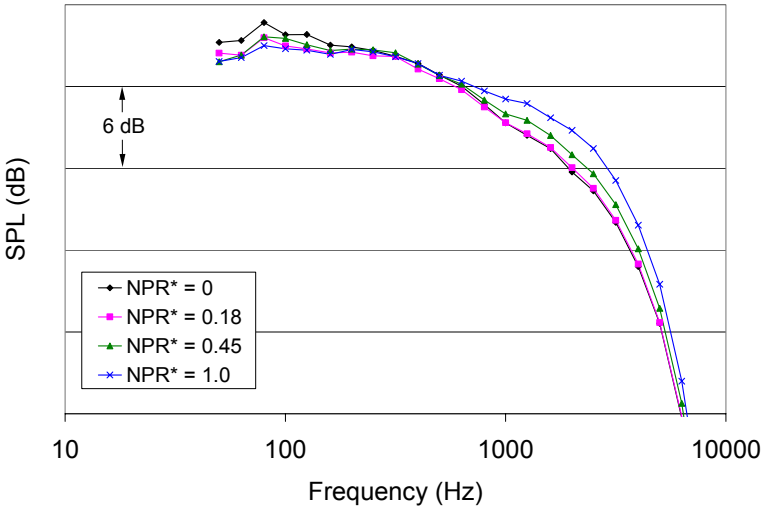

Figure 11 SPL spectra of 8I nozzle operating at cycle point 15, Mfj = 0.10, θ = 60°.

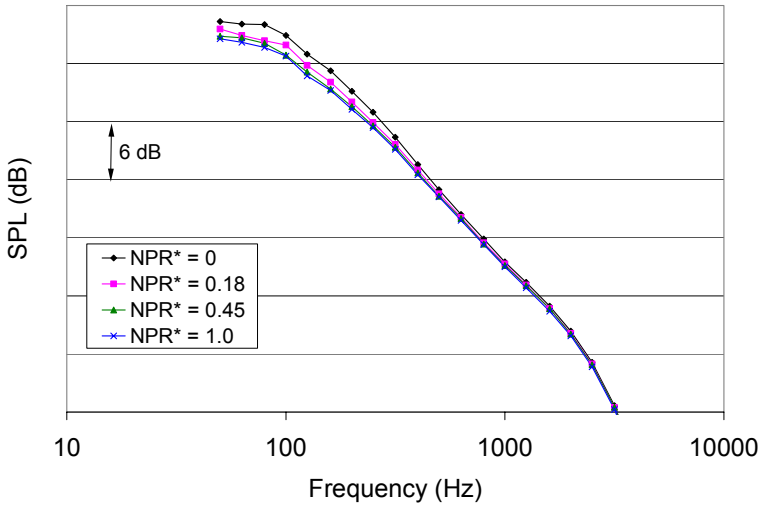

Figure 9 SPL spectra of 8I nozzle operating at cycle point 15, Mfj = 0.10, θ = 145°.

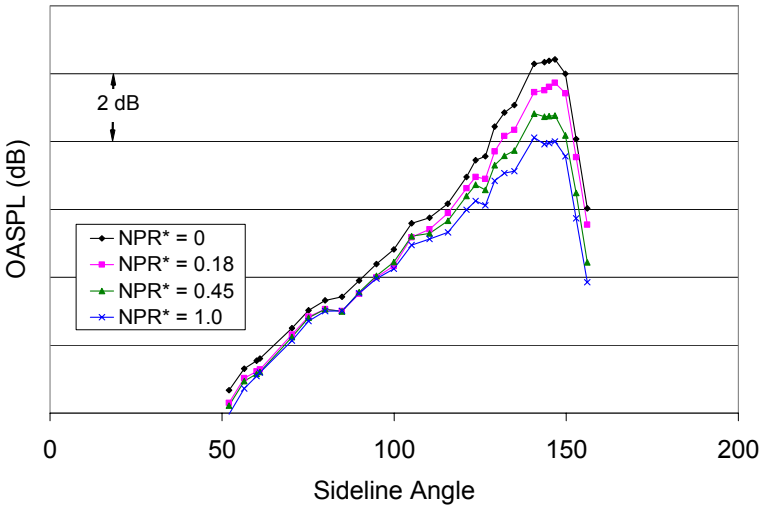

Figure 12 OASPL of 6I nozzle operating at cycle point 15, Mfj = 0.10.

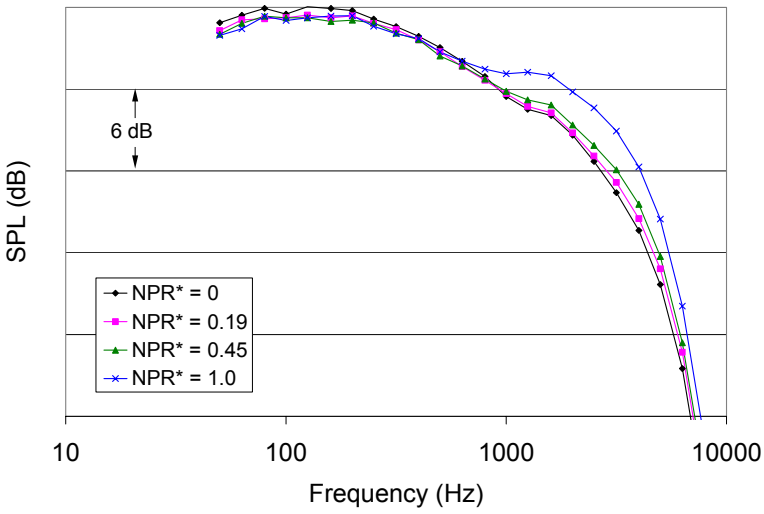

Figure 10 SPL spectra of 8I nozzle operating at cycle point 15, Mfj = 0.10, θ = 90°.

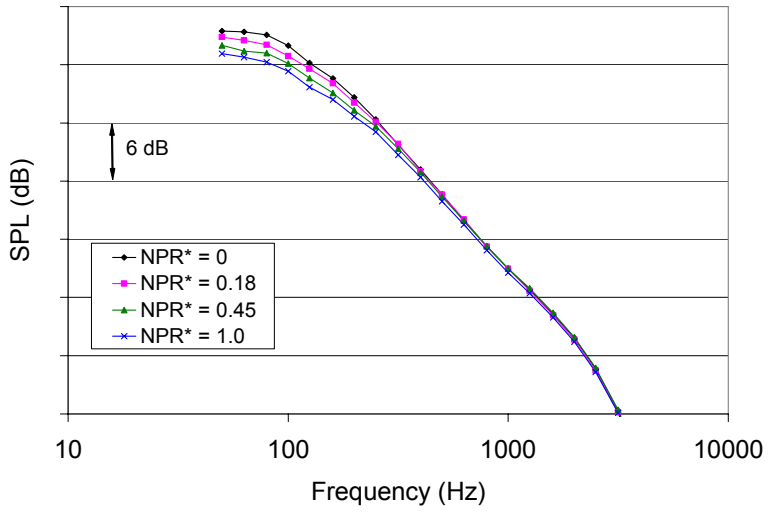

Figure 13 SPL spectra of 6I nozzle operating at cycle point 15, Mfj = 0.10, θ = 145°.

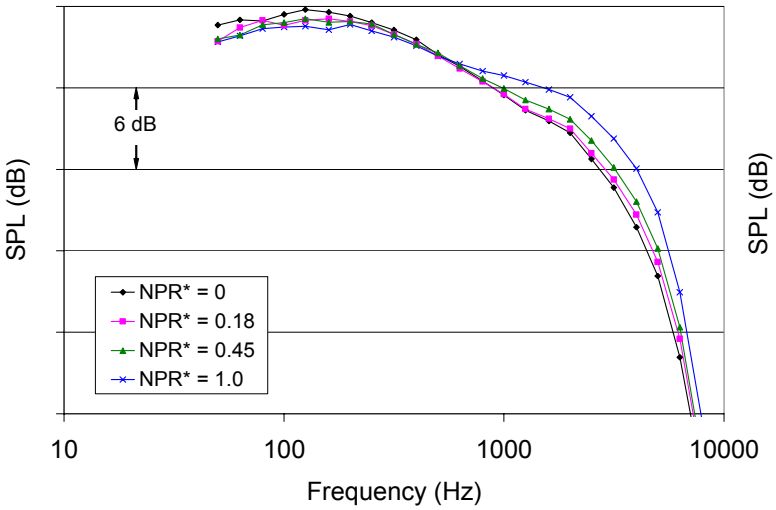

Figure 14 SPL spectra of 6I nozzle operating at cycle point 15, Mfj = 0.10, θ = 90°.

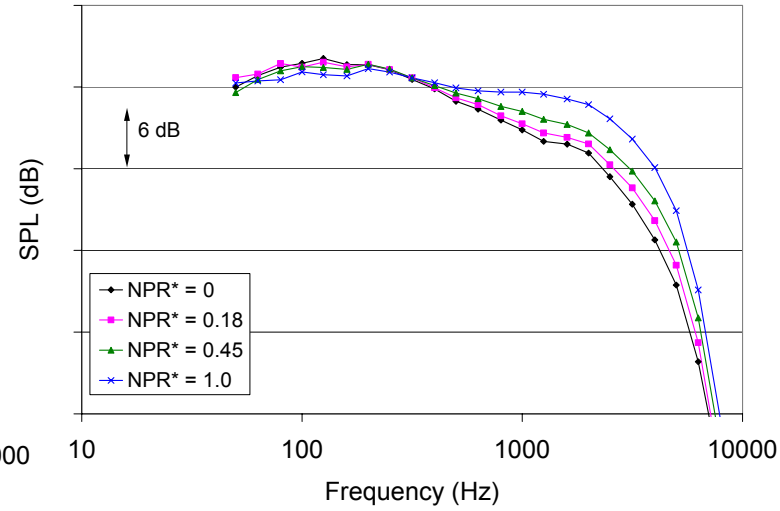

Figure 17 SPL spectra of 6I nozzle operating at cycle point 15, Mfj = 0.28, θ = 90°.

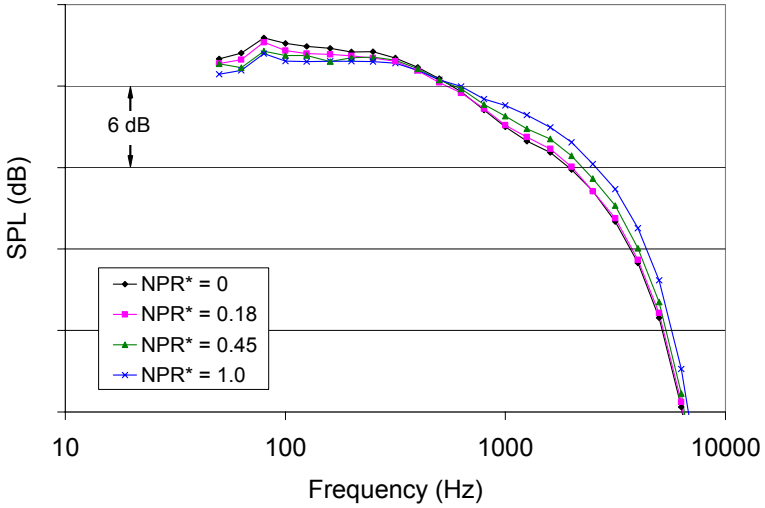

Figure 15 SPL spectra of 8I nozzle operating at cycle point 15, Mfj = 0.10, θ = 60°.

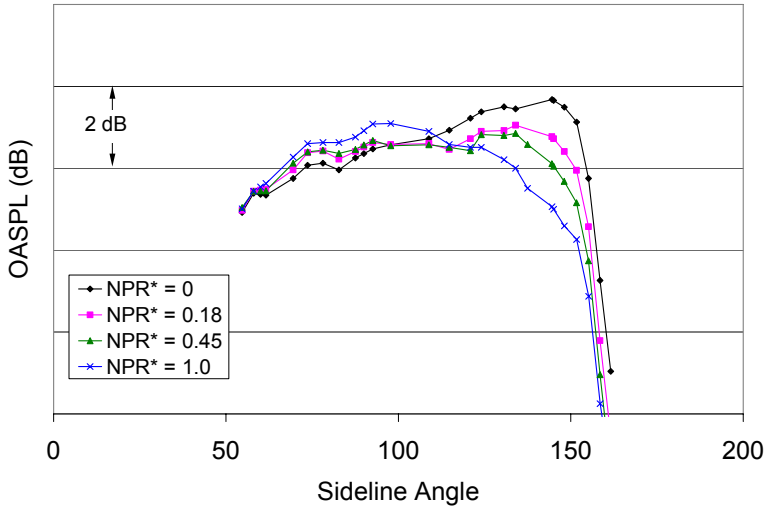

Figure 16 OASPL of 6I nozzle operating at cycle point 15, Mfj = 0.28.